https://doi.org/10.5194/egusphere-2026-2924
Preprint. Discussion started: 26 June 2026

A Weakly Supervised Deep Learning Framework for Estimating Above-Ground Biomass for Non-Forest Landscapes From Optical Images

Rachel Nubwimana[1], Martin Brandt[1], Philippe Ciais[2], Maurice Mugabowindekwe[1, 6], Sizhuo Li[1], Andrew Davies[3], Dimitri Gominski[1], Rasmus Fensholt[1], Sassan Saatchi[4], and Fabian Gieseke[5]

[1]Department of Geosciences and Natural Resource Management, Geography, Land, Environment and Society University of Copenhagen, 1350 København K
[2]Laboratoire des Sciences du Climat et de l'Environnement, LSCE/IPSL, UMR CEA-CNRS-UVSQ 8212
[3]Department of Organismic and Evolutionary Biology, Harvard University Cambridge, MA 02138, USA
[4]Institute of the Environment and Sustainability, University of California, 619 Charles E. Young Drive East, Los Angeles, CA 90095
[5]Department of Information Systems, University of Münster, Leonardo-Campus 3, 48149 Münster, Deutschland
[6]Rwanda Space Agency, KG 17 Ave, Remera Hallmark Center, Kigali, Rwanda

Correspondence: Rachel Nubwimana (nubw@ign.ku.dk)

Abstract. Above-ground biomass (AGB) maps are essential for carbon accounting and sustainable land management, yet AGB for non-forest landscapes remains poorly accounted for in global datasets. Here, we make use of deep learning and high-resolution PlanetScope imagery to introduce the concept of AGB contribution maps, which are high-resolution AGB predictions that capture local patterns. These maps can be predicted at any resolution from 1 to 100 m, providing insights into the spatial features included in the coarser resolution AGB maps, being essential for mapping trees outside forests. Our method employs a weakly supervised hybrid framework that transfers information from an existing 100 m global AGB map to high-resolution optical satellite imagery, enabling the interpretation of detailed spatial patterns. We demonstrate that our map achieves detailed and spatially consistent patterns of woody vegetation in African savanna landscapes comparable to UAV-based LiDAR. Aggregated AGB values are well aligned with independent in-situ measurements ($r2 = 0.71$, bias 1%), which is contrary to the original coarse AGB map used for training ($r2 = 0.17$, bias 48%), indicating the capability of our approach to refine the existing map towards a higher accuracy for estimating tree biomass outside forests. This suggests that our model has learned tree-level information that is not present in the original AGB training data, providing a framework to refine existing coarse-resolution AGB maps. The granular and multi-resolution results provide no contribution to global efforts in sustainable land management of non-forest landscapes at any preferred scale and resolution.

1 Introduction

Accurately mapping AGB, including in non-forest landscapes, is critical for understanding the global carbon cycle, improving CO_2 emission estimates, and developing climate change mitigation strategies. Data and information on AGB play a key role in assessing carbon sequestration and refining deforestation-related emission models (Saatchi et al., 2011), (Baccini et al.,

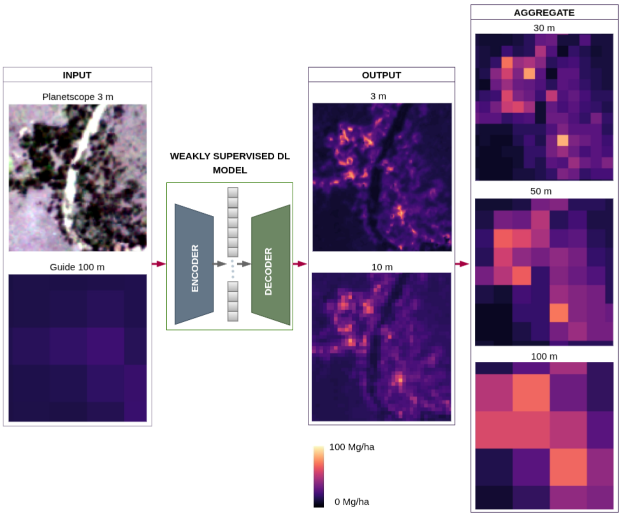

Figure 1. Graphical workflow of the weakly supervised deep learning model for high-resolution AGB mapping. PlanetScope 3 m imagery is used as input, with a 100 m AGB map as the source of weak supervision. The encoder-decoder network is trained to predict AGB contribution maps at any desired resolution (e.g. 3 m or 10 m that can subsequently be aggregated to 30 m, 50 m, or 100 m). The color scale represents the AGB density of this small area (0-100 Mg/ha).

2012). While forested areas have been the primary focus of AGB research, non-forest landscapes, such as savannas, shrublands, and drylands have historically been understudied (Cunliffe et al., 2022). These ecosystems contribute substantially to carbon storage and ecological functions, yet their AGB distribution remains poorly characterized due to a lack of detailed mapping approaches (Shi et al., 2021). The lack of detailed AGB maps in these landscapes impedes accurate carbon accounting and ecosystem restoration planning. Overcoming this requires advanced mapping approaches that are able to accurately capture the spatial AGB variability of different non-forest ecosystems. Large-scale AGB mapping efforts largely rely on remote sensing technologies that upscale field-measured AGB. Optical satellite sensors, such as Landsat and Sentinel-2, have been widely used for AGB estimation, primarily through relating spectral values and vegetation indices to AGB distribution (H. Nguyen et al., 2019). However, these indices tend to have reduced sensitivity in non-forest ecosystems due to a high influence of soil reflectance, mixed woody-herbaceous structures, and low vegetation density, making them less reliable in such landscapes. Additionally, optical remote sensing data are affected by atmospheric perturbations, particularly cloud cover and aerosol contamination, which can compromise data quality and lead to uncertainties. The integration of complementary remote sensing data sources such as information from synthetic aperture radar (SAR) and spaceborne LiDAR have improved AGB estimations (Schwartz et al., 2023), (Lang et al., 2023), (Pauls et al., 2024). SAR provides structural insights independent of atmospheric conditions, making it particularly useful for AGB estimation (Santoro and Cartus, 2018). However, SAR backscatter is highly sensitive to local topography, soil moisture variations and vegetation structure, requiring careful calibration. Complementing SAR, LiDAR, particularly from the Global Ecosystem Dynamics Investigation (GEDI) mission, provides detailed structural measurements, capturing canopy height and vertical vegetation profiles with a spatial resolution of about 30 m. These structural metrics enhance AGB estimation when integrated with allometric models that apply ground calibration data to convert satellite derived metrics into biomass (Chave et al., 2014), (Duncanson et al., 2022). Nevertheless, GEDI derived biomass maps are typically produced at resolutions $>$ 30-100 m, which is sufficient for forest biomass estimations, but does not provide adequate information on trees outside forests. This limits its effectiveness for large-scale continuous biomass mappings in non-forest ecosystems, where vegetation is fragmented and structurally mixed (Li et al., 2023b), (Li et al., 2024). One of the challenges to estimating AGB in non-forest ecosystems at large scale is the limited availability of high-resolution local training data such as LiDAR, extensive field-based measurements, and geolocation uncertainties associated with spaceborne instruments like GEDI. These combined limitations represents an important shortcoming for calibrating and validating biomass estimation models (Wang et al., 2024). Traditional decision tree-based machine learning models like random forest often fail to capture the complex spatial dependencies in heterogeneous landscapes such as drylands, savannas, and shrublands (Lu et al., 2016). Although previous studies have explored multi-sensor fusion techniques that integrate optical, SAR, and LiDAR data to improve biomass predictions (Wang et al., 2024), these approaches often rely on manually engineered features and statistical models, which limit their scalability and generalization across diverse landscapes (Fassnacht et al., 2014). As a result, current global AGB maps are generally consistent and homogeneous, but fail to capture the complex non-forest vegetation structure, in particular in tropical environments. On the other hand, local-scale maps provide more spatial details but remain difficult to scale and require LiDAR and field data, which are often not available for non-forest regions. Deep learning has emerged as a powerful method for remote sensing analysis, with demonstrated ability to capture spatial structures and learning multi-sensor dependencies from high-resolution remote sensing data (Li et al., 2022). In fully supervised settings, convolutional neural networks and attention-based models, in particular, have proven highly effective in extracting hierarchical features that can be used to map canopy height from GEDI and Sentinel-2 or higher resolution sensors (Lang et al., 2023), (Pauls et al., 2024), which can be used to improve AGB predictions (Wang et al., 2024). Moreover, super-resolution techniques including Generative Adversarial Networks (GANs) and transformer-based architectures have shown promise for refining coarse AGB estimates and improving spatial resolution (Li et al., 2023a), (Leonhardt et al., 2022). Despite these advancements, resolving the scale mismatch between coarse AGB maps and small woody features remains a challenge, particularly in non-forest ecosystems. Advances in computer vision have shown the potential of weakly supervised learning, where models can be supervised with coarse-resolution or incomplete labels, and learn to produce enhanced outputs by exploiting spatial and temporal correlations between datasets (Leonhardt et al., 2022), (Kang et al., 2024). Given the current availability of global AGB maps and global-coverage high-resolution satellite imagery, this approach holds promise for improved AGB mapping and has also been referred to as a guided super-resolution for AGB (Karaman et al., 2025). Building on these insights, we developed a weakly supervised learning method for AGB mapping from existing coarse-resolution products, while exploiting the spatial details in high-resolution satellite images. The aim of the study is to refine existing coarse resolution maps towards an improved performance for complex non-forest landscapes using optical high-resolution images. This framework uses coarse-resolution AGB labels that provide limited guidance during training. Unlike fully supervised super-resolution methods, which learn a mapping to fine-scale patterns from their low-resolution equivalents, our approach makes use of spectral features from optical imagery to infer missing spatial details, without depending on high-resolution local datasets such as LiDAR or field-based measurements. To implement this learning process, we introduce the concept of an AGB contribution map, representing an intermediate high-resolution prediction output that encourages the model to learn detailed spatial patterns that can subsequently be aggregated to match coarser resolution AGB targets at any desired resolution. Our approach focuses on generating AGB contribution maps using 3 m resolution optical satellite imagery as input and existing 100 m resolution AGB maps as labels. Before regressing the coarse-resolution AGB grids, the model first predicts an intermediate representation at 3 m to 10 m resolution, referred to as the AGB contribution map in Fig. 1, which captures high-resolution spatial variability in AGB distribution, such as for trees outside forests. This representation allows the model to fully exploit the spatial patterns available in high-resolution imagery while ensuring that predictions remain consistent with coarse resolution reference data. The AGB contribution map can be aggregated to generate AGB maps at any desired spatial resolution (e.g. 30 m, 50 m, or 100 m), supporting integration with existing large-scale AGB products, while preserving local structural details, see Fig. 1. This framework enables detailed AGB estimation at a high spatial resolution, even in non-forest areas where woody vegetation is sparse or unevenly distributed. Therefore, it offers a scalable solution for mapping high-resolution AGB in landscapes where such information has historically been unavailable or incomplete.

2 Methods

This study introduces a scalable deep learning framework for estimating AGB in non-forest landscapes (i.e non contiguous canopies) using high-resolution PlanetScope nano-satellite imagery, hereafter referred to as Planet, and weak supervision. The AGB contribution map features how AGB is distributed within widely-used AGB measurement units (coarse scale grid cells), such as 1 hectare (100x100 m), particularly allowing to account for scattered non-forest woody vegetation. Traditional AGB mapping approaches rely predominantly on extensive field plot measurements or airborne LiDAR, both of which are limited in spatial extent and coverage in mixed, open-canopy ecosystems. Our approach bypasses these limitations by training only on globally available coarse-resolution AGB maps, while learning the spatial details captured by the high-resolution satellite images. This framework comprises four key components: (1) systematic preprocessing of Planet data, (2) a deep encoder-decoder neural network architecture optimized for spatial details, (3) a model training paradigm that allows high-resolution learning from coarse supervision, and (4) a resolution-adaptive inference strategy for generating multi-scale AGB maps. Together, these components enable a refined and generalizable AGB estimation for areas outside contiguous forests.

2.1 Study Area

The proposed framework was trained across Tanzania (947,300 km^2), and Rwanda (26,338 km^2) (see Supplementary Figure S1). Although AGB estimates were generated continuously at national scale, the scope of this analysis focuses on non-forest ecosystems. These target landscapes cover diverse open-canopy systems including savannas, shrublands, drylands, and agro-forestry systems, characterized by fragmented patterns of woody vegetation, mixed land use, and a high dominance of trees outside forests. The study area extends across diverse topographic, climatic, and ecological zones, including variations in elevation, precipitation, soil characteristics, and land cover types. This environmental heterogeneity offers a foundation for evaluating the model's capacity to produce spatially consistent, resolution-adaptive AGB estimates under weak supervision. It also enables assessment of how well the framework generalizes across structurally and spectrally diverse landscapes without requiring local field-based calibration. The ecosystems targeted contribute significantly to regional carbon storage, climate resilience, and biodiversity (Veldman et al., 2015). However, they remain underrepresented in most large-scale AGB mapping efforts (Bouvet et al., 2018), (Tucker et al., 2023), which have historically focused on dense, closed-canopy forest biomes (Spawn et al., 2020). The vegetation in these regions are often sparsely and irregularly distributed, with sharp spatial transitions between vegetated and non-vegetated areas (Cunliffe et al., 2022), (Nghiyalwa et al., 2021). Such structural characteristics remain a challenge to conventional AGB estimation methods, particularly those relying on medium-resolution optical or radar imagery that lacks the spatial details to resolve small woody features (Shi et al., 2021). Furthermore, the mixed spectral signals in the imagery caused by combinations of tree cover, grass, bare soil, and agricultural activity reduce the reliability of traditional vegetation indices and regression-based models for estimating AGB (Liu et al., 2021). These limitations are particularly evident in open-canopy, non-forest regions, where strong soil reflectance and pixel-level mixing make it difficult to accurately separate vegetation and background signals in medium-resolution imagery that remains to be the most commonly used remote sensing data for large-scale AGB mapping efforts (Nghiyalwa et al., 2021), (Yan et al., 2025). Approaches for estimating AGB of single trees in this area require expensive sub-meter resolution images and only perform well if tree crowns are clearly visible, which may not be the case in shrublands and young plantations (Tucker et al., 2023), (Mugabowindekwe et al., 2023).

2.2 Remote Sensing Data

We use Planet imagery acquired in 2019, covering the full extent of Tanzania and Rwanda. The dataset consists of blue, green, red, and near infrared bands captured daily at approximately 3 m spatial resolution (Planet Labs PBC, 2022). We preprocessed Planet imagery 1x1 degree mosaics derived from raw scenes accessed via the PSScene item type and the ortho-analytic-4b-sr asset, an atmospherically corrected surface reflectance product. The preprocessing followed the acquisition and compositing strategy described by (Reiner et al., 2024), which includes metadata-based scene filtering, phenology-informed temporal selection derived from MODIS-based vegetation phenology data, and radiometric harmonization via histogram matching with Landsat reference imagery. We refer to (Reiner et al., 2023) for details on the data processing. Following data preprocessing, the mosaics were tiled into non-overlapping 100×100 m patches. Each tile was resampled to 1m using bilinear interpolation to enable the learning of details at high-resolution prediction, and flexible aggregation of results at multiple scales after prediction. Although the resampling does not increase the native spatial resolution of the imagery, it facilitates pixel-level modeling of high-resolution vegetation structure within each coarse AGB unit.

2.3 Reference AGB Map

The labels used for model training were derived from the 2020 AGB map of Africa, produced by (Xu et al., 2021). This map provides spatially continuous AGB estimates at 100 m resolution across the continent and has been utilized in several studies addressing AGB distribution and carbon monitoring in African landscapes (Bouvet et al., 2018), (Wan et al., 2025). (Xu et al., 2021) generated the map using a supervised machine learning approach trained on footprint-level above-ground biomass density (AGBD) estimates from the GEDI Level 4A product (Dubayah et al., 2020). These estimates were derived from full-waveform LiDAR data and served as the target variable in a predictive model. The input predictors included; Backscatter metrics from Sentinel-1 (C-band) and ALOS-2 PALSAR (L-band) to characterize vegetation structure, MODIS Vegetation Continuous Fields (percent tree cover) (MODIS VCF), Landsat-derived Forest cover loss and canopy metrics (Hansen et al., 2013), SRTM elevation and generalized climate layers to account for environmental variation. Model training was supported by a harmonized dataset of forest inventory plots from various countries, and forest types, which were used to help calibrate biomass prediction in conjunction with the GEDI-derived AGBD estimates (Xu et al., 2021). It is important to note that this reference map itself is the product of a machine learning model rather than a direct field measurement. As such, the labels used in this research are both coarse in resolution (100 m) and potentially noisy.

2.4 Deep Learning Model and Training Strategy

To predict AGB contribution maps at high-resolutions (e.g., 10 m), where each pixel represents its relative contribution to the total AGB within a 100x100 m input tile, we developed a hybrid encoder–decoder convolutional neural network trained under weak supervision. The model was then trained on Planet imagery with the corresponding 100 m AGB labels from the reference map. The model is designed to extract hierarchical spatial features, enabling high-resolution predictions in structurally complex, non-forest landscapes.

2.4.1 Network architecture

The network adopts an encoder-decoder structure combining a ResNet50 backbone (He et al., 2016) with a UNet-style decoder (Ronneberger et al., 2015), enhanced with additive attention gates (Oktay et al., 2018). The encoder consists of a ResNet50 pretrained on ImageNet, which extracts multiscale feature representations from the input Planet imagery. Feature maps from selected encoder layers are retained as skip connections to preserve spatial details and contextual information during decoding. The decoder reconstructs dense spatial outputs via transposed convolutions, integrated with skip connections and attention modules that selectively emphasize semantically relevant regions such as tree crowns and clustered vegetation, while suppressing background artifacts like bare soil or infrastructure. Each decoding block includes convolutional layers followed by batch normalization and layer normalization to ensure stable convergence and retention of fine details. The final output is a single-channel per-pixel prediction of AGB contribution, generated via a 1×1 convolutional head.

2.4.2 Weak supervision via spatial pooling

Training labels were derived from the 2020 AGB map of Africa (Xu et al., 2021) that provides AGB estimates at a spatial resolution of 100 m. We adopted a weak supervision strategy in which each 100×100 m Planet imagery with an upsampled resolution of 1 m is paired with a single scalar AGB value $y_{\text{agg}} \in \mathbb{R}$ as a target, where y_{agg} represents the mean AGB (in megagram, Mg) within a tile. In this case, the model assumes that the target scalar value is the mean AGB within 100×100 m, and therefore, areas with high AGB within the image (e.g. pixels covered by tree crowns) would have high influence on the activation map.

The model is then trained to produce an AGB contribution map $\hat{y} \in \mathbb{R}^{H \times W}$ where $H = W = 100$ corresponding to $100\,\mathrm{m} \times 100\,\mathrm{m}$ tile at input spatial resolution (i.e. 1 m resolution). Each prediction $\hat{y}_{i,j}$ denotes the estimated contribution at pixel (i,j).

To compute the predicted scalar value corresponding to the reference label, we apply a spatial mean pooling to aggregate the dense prediction:

$$\hat{y}_{\text{agg}} = \frac{1}{H \cdot W} \sum_{i=1}^{H} \sum_{j=1}^{W} \hat{y}_{i,j} \tag{1}$$

Here, $\hat{y}_{i,j}$ is the predicted contribution value at a 1 m pixel (i,j), and H and W denote the height and width of the tile in pixels, respectively. The training objective minimizes the Mean Absolute Error (MAE) between the aggregated prediction and the reference AGB label:

$$LMAE = \frac{1}{N} \sum_{n=1}^{N} \left| y_{\text{agg}}^{(n)} - \hat{y}_{\text{agg}}^{(n)} \right| \tag{2}$$

Here, MAE is the Mean Absolute Error, N is the number of training tiles. This formulation constrains the network to spatially distribute AGB in a way that preserves consistency with the total AGB observed at the coarse scale of 100 m. By exploiting spectral and spatial texture signals present in the high-resolution imagery, the model learns to reconstruct AGB patterns in the absence of pixel-level ground truth. This ultimately results in a map at the same resolution of the input Planet imagery, with a pixel value representing the AGB contribution of that specific pixel to the 100×100 m area.

2.4.3 Optimization and pipeline

Training was performed using the Adam optimizer by (Kingma and Ba, 2017) with an initial learning rate of 0.001, L2 regularization by (Ng, 2004), and He normal initialization of model parameters. Early stopping was applied based on the validation Mean Absolute Error (MAE), terminating training when the validation performance failed to improve over a fixed number of epochs. This strategy helps prevent overfitting and ensures better generalization on unseen data. Hyperparameters were selected via manual tuning on the validation set using a coarse grid search over plausible values (e.g., as learning rate, regularization strength, and early stopping). The combination that yielded the lowest MAE on the validation set was retained. The final performance metrics are reported on both independent hold-out-test, and on an independent dataset that were not used during training or hyperparameter selection. To support large scale training and inference, we developed a custom multiprocessing pipeline to enable efficient large-scale training and inference. This includes data tiling, interpolation, georeferenced image reading and writing, and batch processing. Each patch is assigned a unique spatial identifier to preserve georeferencing during post-processing. This fully integrated workflow ensures scalability, and the ability to generate seamless high-resolution AGB maps across large scales such as national or regional scales.

2.5 Model Training Paradigm

Unlike typical teacher-student models, which assume availability of high-resolution labels or synthetic pseudo-labels, our approach is specifically tailored to operate in label-scarce environments. This weak supervision strategy can effectively cope with the absence of dense, pixel-by-pixel, supervision and is designed to function without any pixel-level supervision. In our setup, the coarse-resolution AGB map acts as a weak global supervisory signal, but it does not provide high-resolution spatial guidance. Instead, the model learns to produce high-resolution AGB contribution maps directly from the high-resolution Planet imagery, guided only by AGB scalar values. This weak supervision setup encourages the network to discover spatial AGB allocation patterns directly from the input imagery by leveraging the spatial richness of spectral reflectance and fine-grained texture available in the Planet imagery. Through its hierarchical feature extraction and attention mechanisms, the model's architecture facilitates the learning of broader contextual cues and vegetation structure. A saliency map analysis (see Supplementary Figure S2) confirms that the model attends ecologically meaningful regions, such as tree crowns and woody vegetation clusters during training, supporting the interpretability and robustness of the learned representations (Simonyan et al., 2013). Unlike pseudo-labeling methods that attempt to replicate dense targets, this weak supervision strategy avoids making assumptions about the spatial fidelity of the supervision, enabling more flexible and robust learning. This model offers the following key benefits: No need for pixel-level labels, the model is trained using coarse resolution labels derived from a machine learning model, which may contain inherent biases and prediction errors. By treating labels as weakly supervisory signals, the model is able to recover high-resolution AGB from high-resolution inputs without overfitting to potentially faulty labels or artifacts. The model learns AGB allocation patterns that generalize across varying spatial resolutions, and the model supports transferability across various, data-scarce environments without requiring localized calibration or dense ground truth see Fig. 2.

2.6 Resolution-Flexible Inference

Once trained, the model produces AGB contribution maps at the native resolution of the input Planet imagery. These high-resolution outputs are designed to be resolution-flexible, thereby enabling spatial aggregation to any coarser grid (e.g., 10 m, 30 m, or 100 m). This flexibility allows the model's predictions to be directly integrated with existing AGB products and monitoring frameworks at various spatial scales. Because the model learns to allocate AGB, it supports a single-model, multi-resolution workflow. This eliminates the need for retraining or scale-specific calibration, facilitating downstream applications in national forest monitoring systems, climate reporting, or land degradation assessments.

2.7 Evaluation

Model evaluation was performed using independent datasets. We selected two UAV LiDAR based datasets; one from Mozambique and one from South Africa (Lautenbach et al., 2026). LiDAR point clouds were converted to canopy height maps at 1 m for both sites. For the site in South Africa, LiDAR data has been converted into plot-level AGB in a previous work, see (Singh et al., 2023).

https://doi.org/10.5194/egusphere-2026-2924
Preprint. Discussion started: 26 June 2026

The evaluation sites fulfill the requirements for independent testing data: First, they use sensors that were not involved in our modelling framework. Second, these areas lie well outside the region from which our model's training data were sampled. Third, the areas are representative of non-forest landscape (savannas with a low to moderate tree density, and a mix of single trees, groups of trees, shrubs and bushes). Fourth, for the site in South Africa, AGB was calculated in a different way using allometric equations at the tree level, which was then aggregated to 20 m plots. The AGB calculation at tree level ensures that it represents individual scattered trees well.

3 Results

3.1 Visual Evaluation

We predict AGB contribution maps at 10 m resolution, which can be aggregated to AGB density maps at any desired resolution. The details in the AGB contribution map provide flexibility to be expressed in either kg or % contribution at the hectare scale, or directly in Mg/ha. For evaluating the model performance, we first predicted an area that has not been seen during training and compared the patterns with UAV based LiDAR data. The area represents a complex savanna region in Mozambique that includes bushes, shrubs and trees of different crown sizes and heights forming irregular patterns (Fig. 2a). The LiDAR campaign was conducted in 2019, and we consequently used PlanetScope data from the same year and period to predict AGB contribution maps. The spatial patterns show that our map can replicate those observed in the UAV-based canopy height map (Fig. 2b-d), with both spatial distribution and magnitude values showing good visual agreement. We also compare our predictions with a recently published 1 m resolution canopy height map by Meta, which shows very similar patterns as our map and the UAV based canopy height map (Fig. 2e) (Tolan et al., 2024). The canopy height map from Sentinel-2/1/GEDI overestimates the overall values (Fig. 2f).

3.2 Quantitative evaluation

We quantitatively evaluated our model trained in Tanzania and Rwanda using UAV LiDAR data from a different campaign in South Africa. UAV LiDAR point clouds were converted to a canopy height map, which was used to segment individual tree crowns. The height and crown area of the trees were used to derive aboveground biomass for 1,215 20x20 m plots using allometric equations, see (Singh et al., 2023). We downloaded Planet imagery for the same time as the field-based measurements were conducted (February 2020), and predicted AGB using our model. The 10-m AGB contribution maps were aggregated to the field plot level with the unit AGB density in Mg/ha. Results indicate good relationships between the independent field data and our predictions at the plot level comparisons ($R^2 = 0.75$; MAE $= 8.6$; bias $= 9\%$) at the 10 m plot level. The strong relationship is evident over the entire value range, almost following the 1:1 regression line, see Fig. 3. Interestingly, when aggregating our map to 100 m and comparing both the original 100 m AGB map used for training and our map aggregated to 100 m with the UAV derived AGB, our map shows an improved relationship with higher correlation values. This demonstrates that the spatial pattern learned at high-resolution is preserved when aggregating to coarser levels, which means that also ag-

https://doi.org/10.5194/egusphere-2026-2924
Preprint. Discussion started: 26 June 2026

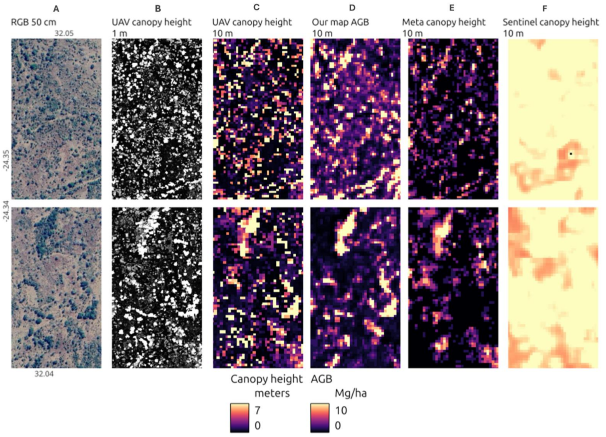

Figure 2. Visual evaluation in a complex landscape. a) We selected a complex savanna landscape in Mozambique, illustrated using Google Earth satellite imagery as visual reference. Imagery © 2024 Airbus, map data © 2024 Google. b) UAV LiDAR based canopy height maps at 1 m and c) aggregated to 10 m. d) Our AGB map predicted at 10 m. e) For comparison purposes, we also include the global Meta canopy height maps from 50 cm Maxar images (Tolan et al., 2024) and f) a state-of-the-art 10-m global canopy height map derived from GEDI and Sentinel-1 and 2 (Pauls et al., 2024). See (Lautenbach et al., 2026) for the exact locations and specifications of the UAV LiDAR data.

gregated AGB maps can benefit from the approach presented here. The original map used for training has a weak relationship ($R^2 = 0.17$) with the UAV data and a high underestimation bias of 48%. When aggregated to 100 m, our map has a considerably higher ($R^2 = 0.71$) and a lower bias -1% at the 100 m plot level. Other AGB maps that have not been particularly designed for non-forest landscapes, such as the ESA CCI map, are unable to map AGB for these areas showing underestimation bias of 91%; and coefficient of determination ($R^2 = -3.3$).

3.3 Application of High-Resolution Maps

In addition to the ability of the high-resolution AGB contribution maps to refine hectare-scale AGB density maps for non-forest areas, there are also a number of applications for the high-resolution maps offering additional insights into ecosystem functioning and services. For example, knowing the exact location of AGB contributions helps clarify how landscape features such as trees in urban areas or in croplands contribute to the region's AGB, in particular where fields are small. We illustrate this Fig. 4, by showing the 10 m resolution contribution to hectare-scale AGB: It is clearly visible how single scattered trees and also groups of trees contribute to the hectare scale AGB (Fig. 4b-d). Calculating the SD within 1x1 hectare grids shows if the distribution of AGB is homogeneous across space, such as in planted forests, or impacted by few scattered trees only Fig. 4. This metric could also provide indications on the woody plant diversity at hectare scale, i.e. if AGB is evenly distributed, such as in monoculture plantations, or more unevenly distributed, such as in a mixed tree-shrub woodland.

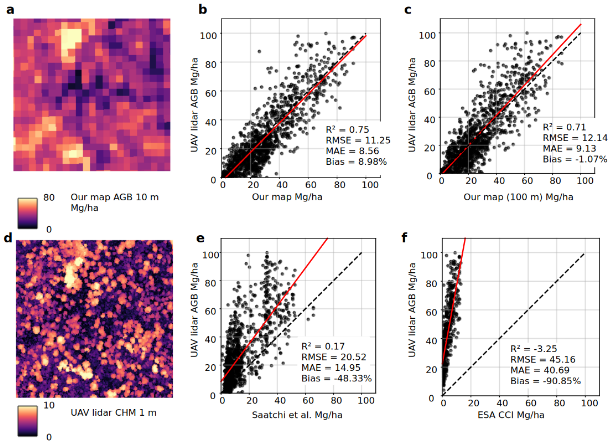

Figure 3. Evaluation with independent UAV data. a) Our AGB predictions at 10 m. b) AGB density from 1,215 20×20 m plots derived from UAV LiDAR observations from Kruger Park, South Africa, used to evaluate AGB predictions at 10 m resolution; all pixels spatially overlapping with the field plots have been averaged for each plot. c) Same as b), but aggregated to 100 m; UAV plot values intersecting the 100 m pixels are used. d) UAV LiDAR canopy height map at 1 m resolution corresponding to the same area as a); the landscape reflects a highly heterogeneous mixture of trees, shrubs, and bushes. e) The original ground truth AGB map at 100 m used for training (Xu et al., 2021), plotted against UAV plot data. f) The ESA CCI biomass map (based on an approach developed for forest areas only), showing no relationship with UAV field data in this savanna landscape. For e) and f), UAV plot values intersecting the 100 m pixels are used. See (Singh et al., 2023) for exact plot locations and AGB calculations.

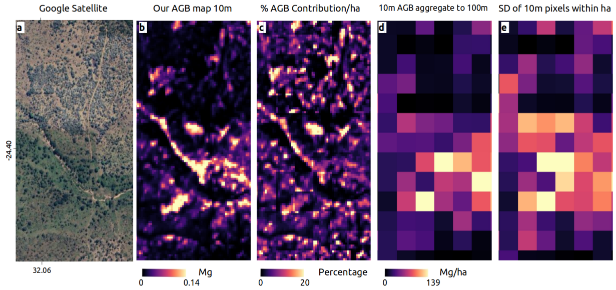

Figure 4. Applications of high-resolution AGB maps. (a) Google Earth satellite imagery used as visual reference. Imagery © 2024 Airbus, map data © 2024 Google, (b) our predicted AGB in Mg/ha at 10 m, (c) the AGB contribution of 10-m pixels to hectare scale AGB in %, (d) an aggregated AGB map at 100 m in Mg/ha, and (e) the SD of 10 m pixels within each hectare, serving as a measure of AGB variations per hectare.

3.4 National-Scale Mapping

To assess national-scale applicability of our approach, we predicted AGB contribution maps for Rwanda at 10 m resolution and aggregated these to 100 m for direct comparison with existing global AGB datasets. All maps were either aggregated to,

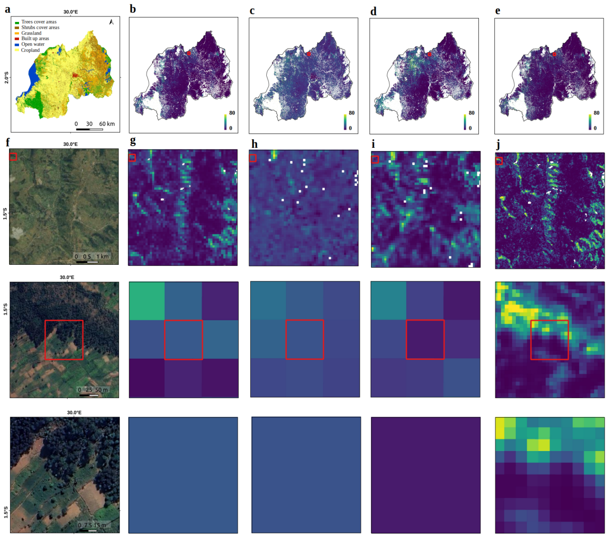

Figure 5. Multi-scale visual comparison of AGB patterns in non-forest landscapes of Rwanda. Forests and open water were masked out in all products prior to comparison. (a) Land-cover map showing the non-forest classes preserved in the analysis. (b-d) National-scale AGB maps at 100 m resolution from our map, (Xu et al., 2021), and (Santoro and Cartus, 2024), respectively. (e) Our national scale AGB map at 10 m resolution. (f) Google Earth satellite imagery used as visual reference. Imagery © 2024 Airbus, map data © 2024 Google, and (g-j) the corresponding local subset. The lower rows provide successive enlargements of the red boxed regions for visual comparison of spatial structure across products.

or produced at 100 m resolution. Forested pixels (land cover class 1 from ESA CCI Land Cover 2016) were excluded from further analysis, to focus on non-forest landscapes given the scope of the study, see Fig. 5 and 6. We compared our predictions with two widely used continental and global-scale AGB products: The ESA CCI AGB from 2019 (Santoro and Cartus, 2024) and the map used to train our model (Xu et al., 2021). We also included two maps specifically produced for Africa (Bouvet et al., 2018) and (Hanan et al., 2020). Comparing approximately 2.1 million non-forest valid pixels at 100 m resolution, there is only moderate and weak statistical agreement between our map and the reference maps as shown in Table 1, reflecting the fact that global AGB products often diverge substantially even over similar landscapes.

To reduce spatial misalignments and classification boundaries, we also aggregated all products to 1 km. Using the ESA WorldCover 10 m land cover map, we sampled representative locations across major non-forest types (e.g., cropland, shrubland, grassland) and computed total AGB within 1 km × 1 km neighborhoods for each map. As shown in Fig. 6 and Table 1, correlations are stronger, especially for (Xu et al., 2021), but still relatively weak.

To understand how these local differences impact on aggregated AGB values, we stratified AGB estimates by major non-forest land cover types see Table 2. Across all maps, cropland dominates total non-forest AGB, followed by grasslands and shrublands. Our map reports higher total AGB than (Xu et al., 2021) in shrubland (12.7%) and grassland (15.5%), and also

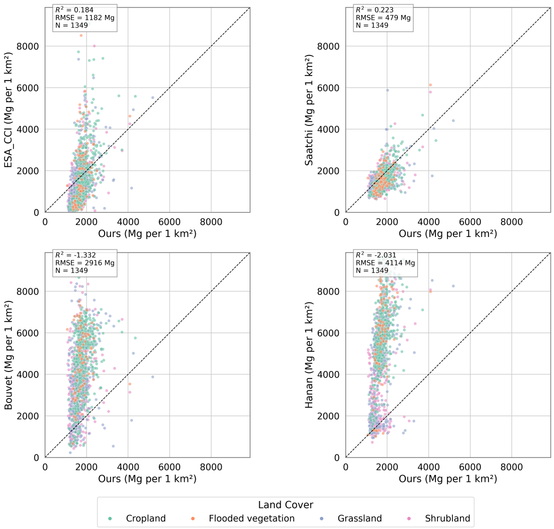

Figure 6. Comparison of 1 km^2 aggregated AGB estimates from our map with four widely used reference products (Santoro and Cartus, 2024; Bouvet et al., 2018; Xu et al., 2021; Hanan et al., 2020) over non-forest landscapes. Each panel presents aggregated AGB densities (Mg km^{-2}), with our estimates shown on the x-axis and the corresponding reference product on the y-axis. Points are coloured by land-cover class (shrubland, grassland, cropland, flooded vegetation, and sparse vegetation), and the dashed line denotes the 1:1 relationship. Coefficients of determination (R^2) reported for each comparison. N = 1349.

in sparse vegetation (25.8%). In contrast, ESA CCI showed slightly higher total AGB in cropland, exceeding our estimate by 0.8%. Our map also has a considerably lower within-class standard deviation as compared to the other products.

4 Discussion

The quantification of non-forest AGB in tropical environments has always been challenging, in particular at a very local scale, such as for smallholder farmlands. Our study proposes a framework that combines publicly available coarse-resolution datasets with low-cost optical imagery. The volume information of the vegetation is learned via the coarse-resolution dataset that has been trained by spaceborne LiDAR (Xu et al., 2021), and the spatial pattern is derived from the optical satellite images. Our work has shown that the model can learn the distribution of AGB across landscape features, such as trees, bushes and shrubs, by itself under a weak supervision concept. Evaluation of our results in a highly heterogeneous landscape has shown that this learned information is closely linked to UAV LiDAR data with almost no systematic bias. This demonstrates that our approach not only generates visually attractive maps but also provides robust and fairly accurate vegetation volume information from optical satellite images at a high-resolution (Singh et al., 2023).

The high spatial resolution of our map gives confidence and clarity in what features are included in the AGB calculations. Predicting at a high spatial resolution provides a high degree of flexibility, allowing to aggregate to any desired spatial reso-

Table 1. Pairwise comparison of AGB maps over Rwanda at 100 m spatial resolution. Statistics are reported for comparisons between the proposed map and existing AGB products, including Xu et al. (2021), Santoro and Cartus (2024), Bouvet et al. (2018), and Hanan et al. (2020). Reported metrics include the coefficient of determination (R^2), root mean square error (RMSE), MAE, bias, mean absolute percentage error (MAPE), and the number of valid pixels (n). All metrics were computed on 100 m raster grids after masking forested areas. Values in parentheses denote the corresponding statistics after aggregation to 1 km spatial resolution.

Our map vs.	R^2	**RMSE (Mg ha^{-1})**	**MAE (Mg ha^{-1})**	**Bias (Mg ha^{-1})**	**MAPE (%)**	**n**
ESA CCI (2019) (Santoro and Cartus, 2024)	0.14	19.16	**13.40**	+0.42	3254.5	2,038,475
	(0.15)	(15.11 / 91%)	**(10.61)**	(+2.96)	(207.17)	(27,008)
Saatchi et al. (Xu et al., 2021)	**0.17**	**11.15**	**6.88**	+1.44	366.1	2,144,928
	(0.42)	**(9.96 / 60%)**	**(5.39)**	(+3.02)	**(38.88)**	(26,919)
Bouvet et al. (Bouvet et al., 2018)	0.03	44.31	29.94	−28.00	63.05	2,149,491
	(0.10)	(41.30 / 36%)	(29.66)	(−28.57)	(56.02)	(27,096)
Hanan et al. (Hanan et al., 2020)	0.16	44.08	37.67	−37.14	63.11	2,097,090
	(0.49)	(47.96 / 31%)	(39.86)	(−39.40)	(62.54)	(26,909)

Bold values indicate the best-performing comparison for each metric.

lution, such as plot or hectare scale. This can be valuable when monitoring the impact on AGB stocks from small scale tree plantations and landscape restoration projects, which often occur outside of contiguous forests and at small scale. Considering that the error is below 10 Mg/ha, multitemporal maps may provide indications on the carbon accumulation of plantations already after a few years of growth. Also at 10 m, our map shows clearly more spatial details than Sentinel-2-based maps that have a ground spacing of 10 m (Pauls et al., 2024).

However, the key output is not the high-resolution of the AGB contribution map. The meaningfulness of high-resolution AGB maps has been subject to debate (Duncanson et al., 2022), but critics mainly concern closed canopy forests. The major achievement is the fact that by aggregating the high-resolution contribution map to the scale of a desired operational AGB map (typically $> 30 \times 30$ m resolution), we show a highly improved relationship with UAV data as compared to previous maps, including the map that has been used for training/supervision (Xu et al., 2021). The reason is that our model is able to make use of the high spatial resolution to assess the importance of scattered trees, shrubs and bushes, and includes their contribution also in aggregated maps, thus being able to correctly quantify the AGB outside contiguous forests.

In this work targeting spatially detailed AGB mapping, we chose to predict AGB directly rather than predicting canopy height, although this would have been possible with the same framework. The conversion of canopy height to AGB requires local field data for allometric equations, which are often not readily available (Chave et al., 2014), (Singh et al., 2023), and the aim was here to test if the model can directly learn and predict volume information (i.e. AGB) instead of vertical information (i.e. canopy height), which has been shown before (Pauls et al., 2024), (Tolan et al., 2024), (Lang et al., 2023), (Schwartz et al.,

Table 2. Comparison of AGB estimates stratified by land cover class across three AGB maps. For each land cover type (Shrubland, Grassland, Cropland, Flooded Vegetation, and Sparse Vegetation), we report the mean AGB (Mg ha^{-1}), standard deviation, number of valid pixels, and total AGB (in Megagrams) per map. AGB maps include our high-resolution prediction ("Our map"), ESA CCI AGB (2019), and Xu et al. (2021). The analysis is based on harmonized 100 m AGB maps clipped to land cover masks from ESA CCI LC v2.1 (2016). All values are computed after forest masking and spatial alignment. Bold values highlight the highest estimates per class.

Land Cover	**AGB Map**	**Mean ± Std (Mg ha^{-1})**	**Total AGB (Mg)**
Shrubland	Our map	14.91 ± 4.48	**4,913,132**
(n = 317,135)	ESA CCI (Santoro and Cartus, 2024)	10.49 ± 13.00	3,033,195
	Saatchi (Xu et al., 2021)	13.30 ± 7.96	4,360,183
Grassland	Our map	18.15 ± 6.77	**10,287,972**
(n = 537,834)	ESA CCI (Santoro and Cartus, 2024)	17.08 ± 18.45	9,316,092
	Saatchi (Xu et al., 2021)	15.98 ± 12.32	8,905,634
Cropland	Our map	18.40 ± 6.00	22,996,315
(n = 1,229,384)	ESA CCI (Santoro and Cartus, 2024)	19.51 ± 22.49	**23,189,693**
	Saatchi (Xu et al., 2021)	17.29 ± 7.82	21,563,925
Flooded Vegetation	Our map	17.35 ± 8.80	**56,220**
(n = 2,879)	ESA CCI (Santoro and Cartus, 2024)	15.52 ± 22.24	45,441
	Saatchi (Xu et al., 2021)	16.40 ± 15.45	40,089
Sparse Vegetation	Our map	21.64 ± 12.31	**3,203**
(n = 132)	ESA CCI (Santoro and Cartus, 2024)	24.33 ± 31.95	2,798
	Saatchi (Xu et al., 2021)	17.32 ± 18.04	2,546

2023). Openly available foundation models, such as DINOv3, require expensive sub-meter images to perform well, while our maps deliver comparable or even improved results from lower cost data available on a daily basis. This allows rapid and frequent AGB assessments, which is an advantage when monitoring restoration and plantation areas.

Our map clearly deviates from existing maps regarding the spatial patterns. These discrepancies are likely driven by differences in input data sources, modeling frameworks, and validation strategies, with ESA CCI (Santoro and Cartus, 2024) optimized primarily for forest AGB, and (Xu et al., 2021) representing a harmonized pan-African product. Although our model was weakly supervised using (Xu et al., 2021) labels, its higher correlation with both reference maps suggests that it may help bridging the gap between existing products by learning spatial AGB patterns that generalize across methods and ecosystems. Aggregated to country level (Rwanda), our map shows 7.5-9.7% higher AGB sums for non-forest landscapes than state-of-the-art products used for comparison. However, the differences expressed in weight units are rather small and sum to an additional 0.00267 Pg as compared to ESA CCI and 0.00338 Pg as compared to (Xu et al., 2021). AGB of non forest landscapes is on average below 20 Mg/ha, and represents a limited carbon sink. Nevertheless, although the impact on national scale numbers is minor, our work has shown that non-forest biomass can be accurately assessed using innovative computer vision methods and low cost satellite data, which is crucial for the management of natural climate solutions providing various ecosystem services to the local population (Veldman et al., 2015), (Spawn et al., 2020).

Code and data availability. The PlanetScope imagery used in this study is available from Planet Labs PBC under licence and cannot be redistributed by the authors. The above-ground biomass products, land-cover products, canopy-height products, and independent validation datasets used in this study are available from the original data providers cited in the manuscript. The derived biomass maps, evaluation outputs, preprocessing scripts, model-training code, inference code, and validation scripts are available from the corresponding author upon reasonable request, subject to the licensing restrictions of the input satellite imagery and third-party datasets.

Author contributions. RN was responsible for conceptualization the study, developed the methodological framework, conducted the analyses, prepared the figures, and wrote the first draft of the manuscript. MB, RF, PC, and FG contributed to the study design, supervision, interpretation of the results, and manuscript revision. SS provided the reference AGB map used for weak supervision and contributed to manuscript revision. MM contributed to the methodological development and interpretation of the Rwanda mapping results and revised the manuscript. AD contributed to the UAV LiDAR-based validation data and its interpretation and revised the manuscript. DG and SL contributed to methodological discussion and manuscript revision. All authors reviewed and approved the submitted manuscript.

References

Baccini, A., Goetz, S. J., Walker, W. S., Laporte, N. T., Sun, M., Sulla-Menashe, D., Hackler, J., Beck, P. S. A., Dubayah, R., Friedl, M. A., Samanta, S., and Houghton, R. A.: Estimated carbon dioxide emissions from tropical deforestation improved by carbon-density maps, Nature Climate Change, 2, 182–185, https://doi.org/10.1038/nclimate1354, 2012.

Bouvet, A., Mermoz, S., Le Toan, T., Villard, L., Mathieu, R., Naidoo, L., and Asner, G. P.: An above-ground biomass map of African savannahs and woodlands at 25 m resolution derived from ALOS PALSAR, Remote Sensing of Environment, 206, 156–173, https://doi.org/10.1016/j.rse.2017.12.030, 2018.

Chave, J., Réjou-Méchain, M., Búrquez, A., Chidumayo, E., Colgan, M. S., Delitti, W. B., Duque, A., Eid, T., Fearnside, P. M., Goodman, R. C., Henry, M., Martínez-Yrízar, A., Mugasha, W. A., Muller-Landau, H. C., Mencuccini, M., Nelson, B. W., Ngomanda, A., Nogueira, E. M., Ortiz-Malavassi, E., Pélissier, R., Ploton, P., Ryan, C. M., Saldarriaga, J. G., and Vieilledent, G.: Improved allometric models to estimate the aboveground biomass of tropical trees, Global Change Biology, 20, 3177–3190, https://doi.org/10.1111/gcb.12629, 2014.

Cunliffe, A. M., Anderson, K., Boschetti, F., Brazier, R. E., Graham, H. A., Myers-Smith, I. H., Astor, T., Boer, M. M., Calvo, L. G., Clark, P. E., Cramer, M. D., Encinas-Lara, M. S., Escarzaga, S. M., Fernández-Guisuraga, J. M., Fisher, A. G., Gdulová, K., Gillespie, B. M., Griebel, A., Hanan, N. P., Hanggito, M. S., Haselberger, S., Havrilla, C. A., Heilman, P., Ji, W., Karl, J. W., Kirchhoff, M., Kraushaar, S., Lyons, M. B., Marzolff, I., Mauritz, M. E., McIntire, C. D., Metzen, D., Méndez-Barroso, L. A., Power, S. C., Prošek, J., Sanz-Ablanedo, E., Sauer, K. J., Schulze-Brüninghoff, D., Šímová, P., Sitch, S., Smit, J. L., Steele, C. M., Suárez-Seoane, S., Vargas, S. A., Villarreal, M., Visser, F., Wachendorf, M., Wirnsberger, H., and Wojcikiewicz, R.: Global application of an unoccupied aerial vehicle photogrammetry protocol for predicting aboveground biomass in non-forest ecosystems, Remote Sensing in Ecology and Conservation, 8, 57–71, https://doi.org/10.1002/rse2.228, 2022.

Dubayah, R., Blair, J. B., Goetz, S., Fatoyinbo, L., Hansen, M., Healey, S., Hofton, M., Hurtt, G., Kellner, J., Luthcke, S., Armston, J., Tang, H., Duncanson, L., Hancock, S., Jantz, P., Marselis, S., Patterson, P. L., Qi, W., and Silva, C.: The Global Ecosystem Dynamics Investigation: High-resolution laser ranging of the Earth's forests and topography, Science of Remote Sensing, 1, 100 002, https://doi.org/10.1016/j.srs.2020.100002, 2020.

Duncanson, L., Kellner, J. R., Armston, J., Dubayah, R., Minor, D. M., Hancock, S., Healey, S. P., Patterson, P. L., Saarela, S., Marselis, S., Silva, C. E., Bruening, J., Goetz, S. J., Tang, H., Hofton, M., Blair, B., Luthcke, S., Fatoyinbo, L., Abernethy, K., Alonso, A., Andersen, H.-E., Aplin, P., Baker, T. R., Barbier, N., Bastin, J. F., Biber, P., Boeckx, P., Bogaert, J., Boschetti, L., Boucher, P. B., Boyd, D. S., Burslem, D. F., Calvo-Rodriguez, S., Chave, J., Chazdon, R. L., Clark, D. B., Clark, D. A., Cohen, W. B., Coomes, D. A., Corona, P., Cushman, K., Cutler, M. E., Dalling, J. W., Dalponte, M., Dash, J., de Miguel, S., Deng, S., Ellis, P. W., Erasmus, B., Fekety, P. A., Fernandez-Landa, A., Ferraz, A., Fischer, R., Fisher, A. G., García-Abril, A., Gobakken, T., Hacker, J. M., Heurich, M., Hill, R. A., Hopkinson, C., Huang, H., Hubbell, S. P., Hudak, A. T., Huth, A., Imbach, B., Jeffery, K. J., Katoh, M., Kearsley, E., Kenfack, D., Kljun, N., Knapp, N., Král, K., Krůček, M., Labrière, N., Lewis, S. L., Longo, M., Lucas, R. M., Main, R., Manzanera, J. A., Martínez, R. V., Mathieu, R., Memiaghe, H., Meyer, V., Mendoza, A. M., Monerris, A., Montesano, P., Morsdorf, F., Næsset, E., Naidoo, L., Nilus, R., O'Brien, M., Orwig, D. A., Papathanassiou, K., Parker, G., Philipson, C., Phillips, O. L., Pisek, J., Poulsen, J. R., Pretzsch, H., Rüdiger, C., Saatchi, S., Sanchez-Azofeifa, A., Sanchez-Lopez, N., Scholes, R., Silva, C. A., Simard, M., Skidmore, A., Stereńczak, K., Tanase, M., Torresan, C., Valbuena, R., Verbeeck, H., Vrska, T., Wessels, K., White, J. C., White, L. J., Zahabu, E., and Zgraggen, C.: Aboveground biomass density models for NASA's Global Ecosystem Dynamics Investigation (GEDI) lidar mission, Remote Sensing of Environment, 270, 112 845, https://doi.org/10.1016/j.rse.2021.112845, 2022.

Fassnacht, F., Hartig, F., Latifi, H., Berger, C., Hernández, J., Corvalán, P., and Koch, B.: Importance of sample size, data type and prediction method for remote sensing-based estimations of aboveground forest biomass, Remote Sensing of Environment, 154, 102–114, https://doi.org/10.1016/j.rse.2014.07.028, 2014.

H. Nguyen, T., Jones, S., Soto-Berelov, M., Haywood, A., and Hislop, S.: Landsat time-series for estimating forest aboveground biomass and its dynamics across space and time: A review, Remote Sensing, 12, 98, 2019.

Hanan, N., Prihodko, L., Ross, C., Bucini, G., and Tredennick, A.: Vegetation Collection, ORNL Distributed Active Archive Center (DAAC) dataset 10.3334/ORNLDAAC/1777 (2020, p. 1777, 2020.

Hansen, M. C., Potapov, P. V., Moore, R., Hancher, M., Turubanova, S. A., Tyukavina, A., Thau, D., Stehman, S. V., Goetz, S. J., Loveland, T. R., Kommareddy, A., Egorov, A., Chini, L., Justice, C. O., and Townshend, J. R. G.: High-Resolution Global Maps of 21st-Century Forest Cover Change, Science, 342, 850–853, https://doi.org/10.1126/science.1244693, 2013.

He, K., Zhang, X., Ren, S., and Sun, J.: Deep Residual Learning for Image Recognition, in: 2016 IEEE Conference on Computer Vision and Pattern Recognition (CVPR), pp. 770–778, IEEE, Las Vegas, NV, USA, ISBN 978-1-4673-8851-1, https://doi.org/10.1109/CVPR.2016.90, 2016.

Kang, X., Duan, P., Li, J., and Li, S.: Efficient Swin Transformer for Remote Sensing Image Super-Resolution, IEEE Transactions on Image Processing, 33, 6367–6379, https://doi.org/10.1109/TIP.2024.3489228, 2024.

Karaman, K., Jiang, Y., Robert, D., Sainte Fare Garnot, V., Santos, M. J., and Wegner, J. D.: GSR4B: Biomass Map Super-Resolution with Sentinel-1/2 Guidance, ISPRS Annals of the Photogrammetry, Remote Sensing and Spatial Information Sciences, X-G-2025, 487–494, https://doi.org/10.5194/isprs-annals-X-G-2025-487-2025, 2025.

Kingma, D. P. and Ba, J.: Adam: A Method for Stochastic Optimization, https://doi.org/10.48550/arXiv.1412.6980, arXiv:1412.6980 [cs], 2017.

Lang, N., Jetz, W., Schindler, K., and Wegner, J. D.: A high-resolution canopy height model of the Earth, Nature Ecology & Evolution, 7, 1778–1789, https://doi.org/10.1038/s41559-023-02206-6, 2023.

Lautenbach, T. C., Radloff, F. G. T., and Davies, A. B.: Using high-resolution remote sensing to quantify nest-site characteristics of White-backed Vultures (*Gyps africanus*) in Karingani Game Reserve, Mozambique, Ibis, 168, 170–181, https://doi.org/10.1111/ibi.13443, 2026.

Leonhardt, J., Drees, L., Jung, P., and Roscher, R.: Probabilistic biomass estimation with conditional generative adversarial networks, in: DAGM German Conference on Pattern Recognition, pp. 479–494, Springer, 2022.

Li, J., Hong, D., Gao, L., Yao, J., Zheng, K., Zhang, B., and Chanussot, J.: Deep learning in multimodal remote sensing data fusion: A comprehensive review, International Journal of Applied Earth Observation and Geoinformation, 112, 102 926, https://doi.org/10.1016/j.jag.2022.102926, 2022.

Li, J., Lv, Q., Zhang, W., Zhu, B., Zhang, G., and Tan, Z.: Multi-Attention Multi-Image Super-Resolution Transformer (MAST) for Remote Sensing, Remote Sensing, 15, 4183, https://doi.org/10.3390/rs15174183, 2023a.

Li, S., Brandt, M., Tong, X., Oehmcke, S., Igel, C., Gieseke, F., Nord-Larsen, T., Fensholt, R., Chave, J., and Ciais, P.: Deep learning tree and forest biomass from sub-meter resolution images, preprint, 2023b.

Li, X., Wessels, K., Armston, J., Duncanson, L., Urbazaev, M., Naidoo, L., Mathieu, R., and Main, R.: Evaluation of GEDI footprint level biomass models in Southern African Savannas using airborne LiDAR and field measurements, Science of Remote Sensing, 10, 100 161, https://doi.org/10.1016/j.srs.2024.100161, 2024.

Liu, J., Maeda, E. E., Wang, D., and Heiskanen, J.: Sensitivity of Spectral Indices on Burned Area Detection using Landsat Time Series in Savannas of Southern Burkina Faso, Remote Sensing, 13, 2492, https://doi.org/10.3390/rs13132492, 2021.

Lu, D., Chen, Q., Wang, G., Liu, L., Li, G., and Moran, E.: A survey of remote sensing-based aboveground biomass estimation methods in forest ecosystems, International Journal of Digital Earth, 9, 63–105, https://doi.org/10.1080/17538947.2014.990526, 2016.

Mugabowindekwe, M., Brandt, M., Chave, J., Reiner, F., Skole, D. L., Kariryaa, A., Igel, C., Hiernaux, P., Ciais, P., Mertz, O., et al.: Nation-wide mapping of tree-level aboveground carbon stocks in Rwanda, Nature Climate Change, 13, 91–97, 2023.

Ng, A. Y.: Feature selection, L_1 vs. L_2 regularization, and rotational invariance, in: Twenty-first international conference on Machine learning - ICML '04, p. 78, ACM Press, Banff, Alberta, Canada, https://doi.org/10.1145/1015330.1015435, 2004.

Nghiyalwa, H. S., Urban, M., Baade, J., Smit, I. P. J., Ramoelo, A., Mogonong, B., and Schmullius, C.: Spatio-Temporal Mixed Pixel Analysis of Savanna Ecosystems: A Review, Remote Sensing, 13, 3870, https://doi.org/10.3390/rs13193870, 2021.

Oktay, O., Schlemper, J., Folgoc, L. L., Lee, M., Heinrich, M., Misawa, K., Mori, K., McDonagh, S., Hammerla, N. Y., Kainz, B., Glocker, B., and Rueckert, D.: Attention U-Net: Learning Where to Look for the Pancreas, https://doi.org/10.48550/ARXIV.1804.03999, version Number: 3, 2018.

Pauls, J., Zimmer, M., Kelly, U. M., Schwartz, M., Saatchi, S., Ciais, P., Pokutta, S., Brandt, M., and Gieseke, F.: Estimating Canopy Height at Scale, https://doi.org/10.48550/ARXIV.2406.01076, version Number: 2, 2024.

Planet Labs PBC: PlanetScope Product Specifications, 2022.

Reiner, F., Brandt, M., Tong, X., Skole, D., Kariryaa, A., Ciais, P., Davies, A., Hiernaux, P., Chave, J., Mugabowindekwe, M., Igel, C., Oehmcke, S., Gieseke, F., Li, S., Liu, S., Saatchi, S., Boucher, P., Singh, J., Taugourdeau, S., Dendoncker, M., Song, X.-P., Mertz, O., Tucker, C. J., and Fensholt, R.: More than one quarter of Africa's tree cover is found outside areas previously classified as forest, Nature Communications, 14, 2258, https://doi.org/10.1038/s41467-023-37880-4, 2023.

Reiner, F., Gominski, D., Fensholt, R., and Brandt, M.: An operational framework to track individual farmland trees over time at national scales using PlanetScope imagery, https://doi.org/10.21203/rs.3.rs-4359628/v1, 2024.

Ronneberger, O., Fischer, P., and Brox, T.: U-net: Convolutional networks for biomedical image segmentation, in: International Conference on Medical image computing and computer-assisted intervention, pp. 234–241, Springer, 2015.

Saatchi, S. S., Harris, N. L., Brown, S., Lefsky, M., Mitchard, E. T. A., Salas, W., Zutta, B. R., Buermann, W., Lewis, S. L., Hagen, S., Petrova, S., White, L., Silman, M., and Morel, A.: Benchmark map of forest carbon stocks in tropical regions across three continents, Proceedings of the National Academy of Sciences, 108, 9899–9904, https://doi.org/10.1073/pnas.1019576108, 2011.

Santoro, M. and Cartus, O.: Research Pathways of Forest Above-Ground Biomass Estimation Based on SAR Backscatter and Interferometric SAR Observations, Remote Sensing, 10, 608, https://doi.org/10.3390/rs10040608, 2018.

Santoro, M. and Cartus, O.: ESA Biomass Climate Change Initiative (Biomass_cci): Global datasets of forest above-ground biomass for the years 2010, 2015, 2016, 2017, 2018, 2019, 2020 and 2021, v5, https://doi.org/10.5285/02E1B18071AD45A19B4D3E8ADAFA2817, artwork Size: 8797 Files, 664510289838 B Pages: 8797 Files, 664510289838 B, 2024.

Schwartz, M., Ciais, P., De Truchis, A., Chave, J., Ottlé, C., Vega, C., Wigneron, J.-P., Nicolas, M., Jouaber, S., Liu, S., Brandt, M., and Fayad, I.: FORMS: Forest Multiple Source height, wood volume, and biomass maps in France at 10 to 30 m resolution based on Sentinel-1, Sentinel-2, and Global Ecosystem Dynamics Investigation (GEDI) data with a deep learning approach, Earth System Science Data, 15, 4927–4945, https://doi.org/10.5194/essd-15-4927-2023, 2023.

Shi, Y., Wang, Z., Liu, L., Li, C., Peng, D., and Xiao, P.: Improving Estimation of Woody Aboveground Biomass of Sparse Mixed Forest over Dryland Ecosystem by Combining Landsat-8, GaoFen-2, and UAV Imagery, Remote Sensing, 13, 4859, https://doi.org/10.3390/rs13234859, 2021.

Simonyan, K., Vedaldi, A., and Zisserman, A.: Deep Inside Convolutional Networks: Visualising Image Classification Models and Saliency Maps, https://doi.org/10.48550/ARXIV.1312.6034, version Number: 2, 2013.

Singh, J., Boucher, P. B., Hockridge, E. G., and Davies, A. B.: Effects of long-term fixed fire regimes on African savanna vegetation biomass, vertical structure and tree stem density, Journal of Applied Ecology, 60, 1223–1238, https://doi.org/10.1111/1365-2664.14435, 2023.

Spawn, S. A., Sullivan, C. C., Lark, T. J., and Gibbs, H. K.: Harmonized global maps of above and belowground biomass carbon density in the year 2010, Scientific Data, 7, 112, https://doi.org/10.1038/s41597-020-0444-4, 2020.

Tolan, J., Yang, H.-I., Nosarzewski, B., Couairon, G., Vo, H. V., Brandt, J., Spore, J., Majumdar, S., Haziza, D., Vamaraju, J., Moutakanni, T., Bojanowski, P., Johns, T., White, B., Tiecke, T., and Couprie, C.: Very high resolution canopy height maps from RGB imagery using self-supervised vision transformer and convolutional decoder trained on aerial lidar, Remote Sensing of Environment, 300, 113 888, https://doi.org/10.1016/j.rse.2023.113888, 2024.

Tucker, C., Brandt, M., Hiernaux, P., Kariryaa, A., Small, J., and Meyers, J.: Vegetation Collection, ORNL Distributed Active Archive Center (DAAC) dataset 10.3334/ORNLDAAC/2117 (2023, p. 2117, 2023.

Veldman, J. W., Buisson, E., Durigan, G., Fernandes, G. W., Le Stradic, S., Mahy, G., Negreiros, D., Overbeck, G. E., Veldman, R. G., Zaloumis, N. P., Putz, F. E., and Bond, W. J.: Toward an old-growth concept for grasslands, savannas, and woodlands, Frontiers in Ecology and the Environment, 13, 154–162, https://doi.org/10.1890/140270, 2015.

Wan, L., Ciais, P., De Truchis, A., Sean, E., Fischer, F. J., Purnell, D., Belouze, G., Fayad, I., Schwartz, M., Xu, Y., Su, Y., Réjou-Méchain, M., Barbier, N., Tresson, P., Bastin, J.-F., Bogaert, J., Vander Linden, A., Plumacker, A., Angoboy Ilondea, B., Assumani, D.-M., De Haulleville, T., Sagang, L. B., Durieux, L., Ryu, Y., Yang, T., Obame, C. V., Bossy, T., Frappart, F., Peaucelle, M., Wigneron, J.-P., Chave, J., Cuni-Sanchez, A., Hubau, W., Verbeeck, H., Boeckx, P., Makana, J.-R., Ewango, C., Kearsley, E., Sonké, B., Libalah, M., and Ploton, P.: Satellite-based mapping of annual canopy height and aboveground biomass in African dense forests, Frontiers in Remote Sensing, 6, 1724 950, https://doi.org/10.3389/frsen.2025.1724950, 2025.

Wang, E., Huang, T., Liu, Z., Bao, L., Guo, B., Yu, Z., Feng, Z., Luo, H., and Ou, G.: Improving Forest Above-Ground Biomass Estimation Accuracy Using Multi-Source Remote Sensing and Optimized Least Absolute Shrinkage and Selection Operator Variable Selection Method, Remote Sensing, 16, 4497, https://doi.org/10.3390/rs16234497, 2024.

Xu, L., Saatchi, S. S., Yang, Y., Yu, Y., Pongratz, J., Bloom, A. A., Bowman, K., Worden, J., Liu, J., Yin, Y., Domke, G., McRoberts, R. E., Woodall, C., Nabuurs, G.-J., de Miguel, S., Keller, M., Nancy, H., Maxwell, S., and Schimel, D.: Dataset for "Changes in Global Terrestrial Live Biomass over the 21st Century", https://doi.org/10.5281/ZENODO.4161694, 2021.

Yan, K., Gao, S., Yan, G., Ma, X., Chen, X., Zhu, P., Li, J., Gao, S., Gastellu-Etchegorry, J.-P., Myneni, R. B., and Wang, Q.: A global systematic review of the remote sensing vegetation indices, International Journal of Applied Earth Observation and Geoinformation, 139, 104 560, https://doi.org/10.1016/j.jag.2025.104560, 2025.